Search for spin-lattice coupling mediated by itinerant electrons: Synchrotron x-ray diffraction and Raman scattering from $GdAl_3$

A. F. García-Flores,[1] A. Malachias,[2] E. Granado,[1,2,*] and Z. Fisk[3]
[1]*Instituto de Física "Gleb Wataghin," UNICAMP, Caixa Postal 6165, 13083-970 Campinas, SP, Brazil*
[2]*Laboratório Nacional de Luz Síncrotron, Caixa Postal 6192, 13083-970 Campinas, SP, Brazil*
[3]*Department of Physics, University of California at Davis, Davis, California 95616, USA*
(Received 25 July 2007; revised manuscript received 14 September 2007; published 15 January 2008)

The coupling among the spin degree of freedom and the atomic displacements in intermetallic $GdAl_3$ was investigated by means of synchrotron x-ray diffraction and polarized Raman scattering. In this compound, the Gd $4f^7$ shell is spherical and the spin-lattice coupling provides a fingerprint of the exchange mechanism and degree of magnetic correlations. X-ray diffraction shows nonresonant symmetry-forbidden charge Bragg peaks below the long-range magnetic ordering temperature $T_N=18$ K, revealing a symmetry-lowering crystal lattice transition associated with Gd displacements, consistent with a Ruderman-Kittel-Kasuya-Yosida mechanism for the magnetic coupling. Raman scattering in fresh broken surfaces shows phonons with conventional frequency behavior, while naturally grown and polished surfaces present frequency anomalies below $T^* \sim 50$ K. Such anomalies are possibly due to a modulation of the magnetic energy by the lattice vibrations in a strongly spin-correlated paramagnetic phase. Such interpretation implies that the spin-phonon coupling in metals may depend on the surface conditions. A fully spin-correlated state immediately above T_N is inferred from our results in this frustrated system.

DOI: 10.1103/PhysRevB.77.024414 PACS number(s): 75.50.Ee, 78.30.Er, 61.05.cp, 63.20.kk

I. INTRODUCTION

The coupling between the lattice and spin degrees of freedom leads to interesting phenomena in condensed matter, such as the colossal magnetoresistance in manganese perovskites,[1] multiferroic behavior in oxides such as RMn_2O_5 and $RMnO_3$ (R=heavy rare earth),[2] and the colossal magnetocaloric effect in $Mn_{1-x}Fe_xAs$,[3] among other examples. The most common mechanisms for spin-lattice coupling are due to interactions between the in-site spin and orbital degrees of freedom, and then between the atomic orbitals and the crystal lattice, leading, for example, to magnetostriction and to the complex spin and orbital patterns in some manganites and other transition-metal oxides. On the other hand, a more direct spin-lattice interaction occurs due to the dependence of the exchange energy on the atomic positions, leading to the so-called exchange striction effect.

To probe the static first-order spin-lattice coupling in crystalline materials, diffraction techniques are becoming increasingly powerful due to the availability of synchrotron x-ray sources, which can detect minute lattice deformations below the spin ordering temperature.[4] However, the spin-lattice coupling can also occur in second order of the atomic displacements, leading to a dynamical effect. This can be probed by the spin-phonon coupling, manifested as an anomalous change in phonon energies with temperature and accessed by either Raman or infrared spectroscopies. Such effect can directly reveal the nearest-neighbor spin correlation $\langle \vec{S}_i \cdot \vec{S}_j \rangle$ and may also provide information on the microscopic mechanism of magnetic coupling.[5–15] Detailed investigations using the spin-phonon coupling have been focused on transition-metal systems, in which the magnetic interactions are believed to be due to d-p-d superexchange interactions in most cases. These interactions are short ranged and extremely sensitive to atomic displacements of the intervening nonmagnetic ions.[5–14] On the other hand, in many metallic systems, the magnetic interactions are commonly mediated by the conduction electrons via the Ruderman-Kittel-Kasuya-Yosida (RKKY) exchange mechanism.[16] In this case, the coupling between RKKY interactions and the crystal lattice is arguably weak and is frequently masked by stronger magnetostriction effects ultimately driven by the spin-orbit interaction.

The title compound [see Fig. 1(a)] is a particularly simple material with Gd^{3+} ions in the $^8S_{7/2}$ ground state having no significant influence of crystal field, single ion anisotropies, or the Kondo effect.[17] In fact, the magnetic moment of a Gd ion has only a spin component. In addition, $GdAl_3$ is of interest because it is one of the end points of the system $Ce_{1-x}Gd_xAl_3$, which shows an interplay of spin-glass and heavy fermion properties.[18,19] Previous studies showed that $GdAl_3$ presents antiferromagnetic ordering at $T_N \sim 18$ K, which is surprisingly low compared with the value of $\theta_{CW} \sim -90$ K.[20,21] The large ratio of $|\theta_{CW}|/T_N \sim 4.9$ is a good indicator of frustrated magnetic interactions, which has been also supported by electron paramagnetic resonance (EPR) measurements.[20] In this paper, we present an anomalous synchrotron x-ray diffraction and Raman scattering study of the first- and second-order spin-lattice coupling in $GdAl_3$. Subtle but fundamentally important effects providing information on the microscopic nature of the magnetism in this compound are described.

II. EXPERIMENTAL DETAILS

A. Sample growth and surface preparation

All single crystals used in the experiments were grown in the same batch from an aluminum melt, as described elsewhere,[20] and are in the form of bars with the long axis

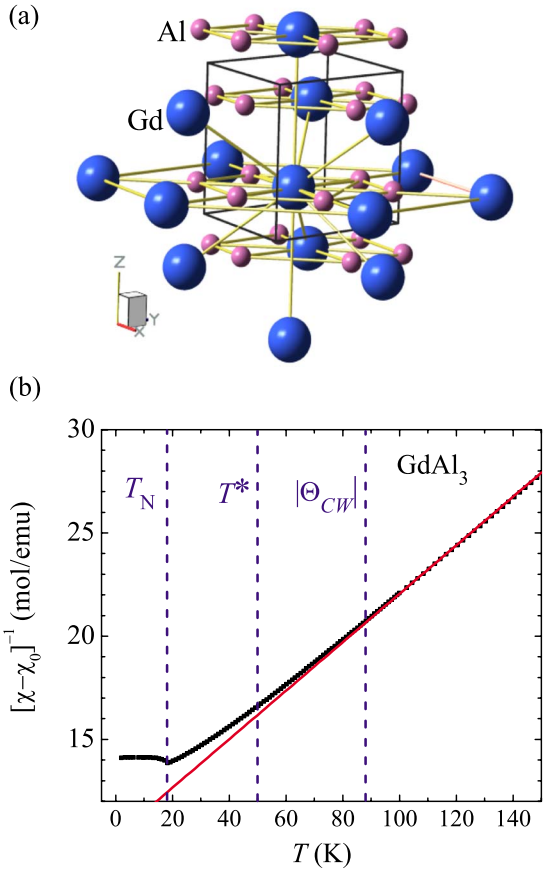

FIG. 1. (Color online) (a) Representation of the crystal structure of hexagonal $GdAl_3$. (b) Inverse magnetic susceptibility $[\chi(T)-\chi_0]^{-1}$ as a function of temperature. The solid line represents an extrapolation of the Curie-Weiss behavior that matches the data between 300 and 790 K (not shown). The vertical dashed lines mark the Néel temperature (T_N), the temperature below which anomalous Raman shifts were observed (T^*), and the modulus of the Curie-Weiss temperature ($|\Theta_{CW}|$).

parallel to the hexagonal c axis (typical dimensions: $1\times1\times3$ mm^3). For the x-ray diffraction experiment, an xz surface with dimensions 1×3 mm^2 was finely polished with alumina powder, yielding a shiny surface with a rocking width of 0.05 full width at half maximum. It was then kept under ambient atmosphere for a few weeks prior to the measurement, with no detectable change in the mosaic width during this period. Unpolished surfaces presented much larger rocking widths and were not employed in our synchrotron x-ray measurements. For the Raman experiments, five crystals were used. For sample named GA1, the same polished xz surface used in x-ray diffraction was employed. This surface was exposed to ambient atmosphere for a few months between the x-ray diffraction and Raman measurements. For the samples named GA2 and GA3, naturally grown xy and xz surfaces were used after being exposed to ambient atmosphere for several months between growth and experiment. The measurements in GA2 were performed a few months before those in GA3. Finally, for samples GA4 and GA5, fresh broken xy surfaces were employed and were kept under vacuum for several hours between the crystal breaking and the Raman measurements. Therefore, the fresh surfaces of samples GA4 and GA5 should represent, most reliably, the bulk behavior of $GdAl_3$ in our Raman measurements.

B. Raman scattering

The Raman scattering spectra were excited with the 514.5 nm laser line from an argon-ion (Ar^+) laser, with a power of ~5 mW. The incident light was focused in a spot of ~100 μm diameter. The scattered light was analyzed by a triple 1800 mm^{-1} grating monochromator system in the subtractive mode equipped with a N_2-cooled charge-coupled device detector. Scattering geometries for the Raman spectra listed in the text and figures follow the usual Porto's notation $A(BC)D$.[22] The measurements as a function of temperature were carried out by mounting the samples on a cold finger of a closed-cycle He refrigerator. All measurements were made in a near-backscattering configuration.

C. Synchrotron x-ray diffraction

The x-ray diffraction measurements were performed on the XRD2 beamline, placed after a dipolar source at the Laboratório Nacional de Luz Síncrotron, Campinas, Brazil. The sample was mounted on the cold finger of a commercial closed-cycle He cryostat with a cylindrical Be window. The cryostat was fixed into the Eulerian cradle of a commercial 4+2 circle diffractometer, appropriate for single crystal x-ray diffraction studies. The energy of the incident photons was selected by a double-bounce Si(111) monochromator, with water refrigeration in the first crystal, while the second crystal was bent for sagittal focusing. The beam was vertically focused by a bent Rh-coated mirror placed before the monochromator, which also provided filtering of high-energy photons (third- and higher-order harmonics). A vertically focused beam was used in our measurements, delivering, at 7.928 keV, a flux of 6×10^{10} photons/s at 200 mA in a spot of ~0.6 mm (vertical) ×2.0 mm (horizontal) at the sample, with an energy resolution of ~5 eV. Our experiments were performed in the vertical scattering plane, i.e., perpendicular to the linear polarization of the incident photons. A solid state detector was used. Reciprocal-space searches for either magnetic or structural forbidden Bragg peaks were performed with the energy set to 7928 eV, very close to the Gd L_{II} edge observed in this compound. A strong enhancement of the magnetic signal is expected for this x-ray energy.[23,24]

III. EXPERIMENTAL RESULTS AND ANALYSIS

A. Magnetic susceptibility

dc-magnetic susceptibility measurements $[\chi(T)]$ were made under a magnetic field of 1 T between 2 and 790 K using a commercial superconducting quantum interference device magnetometer. A fit of the experimental $\chi(T)$ curve in the range $300\ \text{K}<T<790\ \text{K}$ to the expression $\chi(T)=\chi_0+C/(T-\Theta_{CW})$ (not shown) yields $C=8.52(2)$ emu K/mol (Gd) and $\Theta_{CW}=-88(1)$ K. In addition, from the observed paramagnetic Curie constant C, an effective moment of

$8.3\mu_B$/Gd is obtained, which is in good agreement with the expected value for Gd^{3+} ions ($7.94\mu_B$).[25] Since the diamagnetic signal from the addenda was not subtracted in our experiment, the Pauli paramagnetic term was not reliably obtained. Figure 1(b) shows the temperature dependence of the inverse magnetic susceptibility $[(\chi(T)-\chi_0)^{-1}]$. The antiferromagnetic ordering temperature, $T_N=18$ K, is in good agreement with reported values.[20,21] Also, an extrapolation of the Curie-Weiss paramagnetic behavior is displayed. It can be noted that $[\chi(T)-\chi_0]^{-1}$ starts to deviate significantly from the Curie-Weiss behavior at temperatures of the order of $|\Theta_{CW}|$, due to spin correlation effects.

B. X-ray diffraction

At room temperature, $GdAl_3$ shows the hexagonal Ni_3Sn-type crystal structure with space group $P6_3/mmc$ (D^4_{6h}).[26,27] The observed lattice parameters are $a=6.326(1)$ and $c=4.592(2)$ Å, consistent with a previous report.[28] Figure 1(a) shows a view of the crystallographic structure of hexagonal $GdAl_3$. Concerning the distances between magnetic atoms, each Gd atom has six neighboring Gd atoms in consecutive planes along the c axis (three above and three below) at a distance of 4.3 Å, two other Gd atoms in the next plane along the c axis at a distance of 4.6 Å, and six Gd atoms within the same plane at a distance of 6.3 Å. The (hhl) Bragg reflections with odd h and l are forbidden for charge scattering, being therefore suitable for investigations on the possible symmetry lowering at magnetostructural phase transitions. Alternatively, an antiferromagnetic spin structure with propagation vector $\vec{\tau}=(0,0,0)$ would also yield a resonant Bragg peak in this position. For the experimental setup, sample orientation, and x-ray energies employed in our measurements, the only reflection belonging to this family that could be accessed was (3 3 1).

A systematic search for symmetry-forbidden Bragg peaks in reciprocal space was performed at 14 and 25 K. Since $GdAl_3$ orders antiferromagnetically at $T_N=18$ K (see above), any intensity increase on cooling might indicate a possible magnetic or symmetry-lowering charge diffraction effect. Table I summarizes the reciprocal-space scans that were performed in this work. Except at the (3 3 1) position (see below), no extra scattering was found for $T<18$ K in these measurements. Additionally, two-dimensional hk and hl maps were measured (see Fig. 2), revealing an intricate T-independent scattering from extended crystalline defects (see, e.g., Ref. 29). At this point, it is not possible to establish whether such defects are bulk representative or induced by the polishing procedure in GA1.

Figure 3 shows θ-2θ scans around the (3 3 1) symmetry-forbidden Bragg peak at selected temperatures at the Gd L_{II} edge. An asymmetric profile due to spurious multiple beam diffraction can be noticed. Although this contribution depended sensibly on the azimuthal angle, we could not eliminate it for any condition allowed by our experimental setup, and therefore the azimuth was fixed in the condition of minimum intensity. On top of such a spurious contribution, an intrinsic and temperature-dependent signal was observed. This can be mostly clearly identified by taking the difference profile between two selected temperatures (see bottom of Fig. 3). A symmetric contribution to the signal can then be perceived, which can be well fitted by a Gaussian line shape. The temperature dependence of the Gaussian area is given in Fig. 4(a), clearly showing a phase transition at 18.3 K. The inset of Fig. 4(a) shows the transition in more detail. A temperature hysteresis can be perceived in a temperature interval of ~0.1 K, indicating a first-order transition.

The origin of the intrinsic signal at the (3 3 1) Bragg position was further investigated. Figure 4(b) shows the ex-

TABLE I. Summary of 1D reciprocal-space scans performed in this work at 14 and 25 K. Measurements span from initial reciprocal-space positions shown in the second column to the positions of the third column.

Type of scan	Initial (h,k,l)	Final (h,k,l)
h scan	(2 0 0)	(3 0 0)
	(1 2 0)	(2 2 0)
	(2 3 1)	(3 3 1)
k scan	(2 1 0)	(2 2 0)
	(3 0 0)	(3 1 0)
	(3 2 1)	(3 3 1)
l scan	(3 0 0)	(3 0 1)
	(2 2 0)	(2 2 1)
	(2 2 1)	(2 2 2)
	(3 2 0)	(3 2 1)
	(3 3 $\frac{1}{2}$)	(3 3 $\frac{7}{2}$)
Mixed scan	(1 1 0)	(2 2 0)
	(2 2 1)	(3 3 1)
	(3 0 0)	(3 1 1)
	(2 2 2)	(3 3 1)

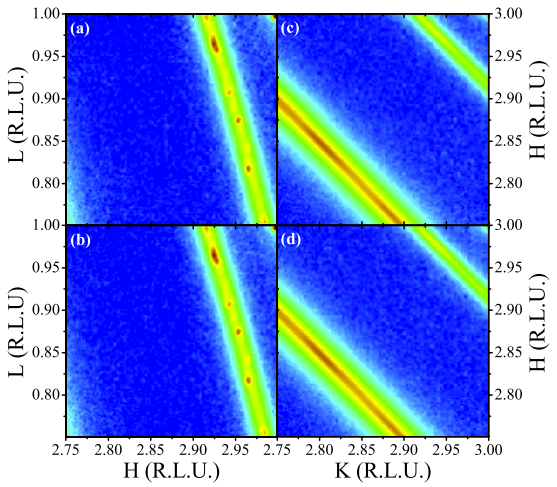

FIG. 2. (Color online) X-ray reciprocal-space maps at the vicinity of the (3 3 1) reflection. (a) hl map at 25 K, (b) hl map at 14 K, (c) hk map at 25 K, and (d) hk map at 14 K. The color intensity scale is linear. The weak observed streaks are associated with extended crystalline defects.

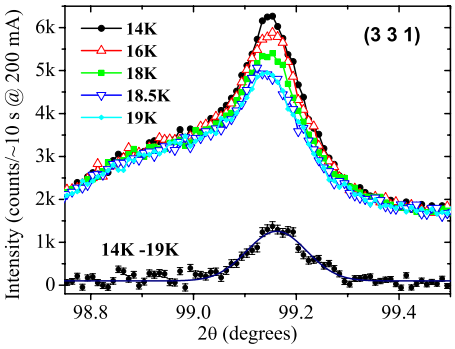

FIG. 3. (Color online) Axial (θ-2θ) scans around the symmetry-forbidden (3 3 1) reflection at selected temperatures, taken with E =7928 eV. A difference profile (symbols) and a fit to a Gaussian (line) are given in the bottom.

perimental structure factor of the (3 3 1) reflection at several energies from 7.88 to 7.98 keV (symbols). The resulting curve clearly displays a minimum at the Gd L_{II} edge. A comparison of this result with the Gd charge scattering factor $f_0+f'(E)$ (Gd) is given in Fig. 4(b) (solid line). To obtain the anomalous Gd dispersion correction f' in this compound, x-ray absorption measurements close to the Gd L_{II} edge were performed in a 35 μm thick $GdAl_3$ membrane, using a grinded sample. Since the anomalous absorption correction f'' is proportional to this measurement, the resulting renormalized spectra can be used to replace tabulated values of f'' close to the edge. The dispersion correction f' of the atomic scattering factor is then directly obtained from the measured f'' via Kramers-Kronig relations.[30] A good agreement between the E dependence of (3 3 1) reflection and $f_0+f'(E)$ (Gd) is observed.

C. Raman scattering

Based on the hexagonal crystal structure and using the method of factor group analysis,[31] the distribution of the degrees of freedom in terms of the irreducible representations of the D_{6h} factor group was calculated and is shown in Table II. According to the character table of the D_{6h} point group, five Raman-active phonon modes ($\Gamma_{Raman}=A_{1g}+E_{1g}+3E_{2g}$) are expected.

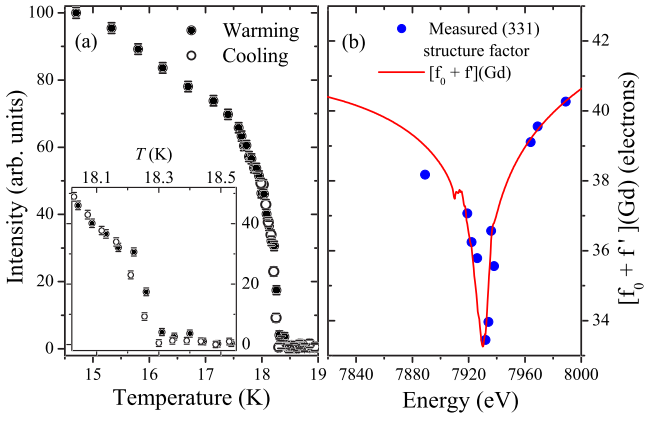

FIG. 4. (Color online) (a) Temperature dependence of the (3 3 1) Bragg peak intensity, defined as the area of the Gaussian line shown in Fig. 3, taken on warming and cooling. The inset shows the same results in an expanded scale close to the transition temperature. (b) E dependence of the (3 3 1) structure factor at 15 K, obtained by the square root of the Bragg peak intensity and normalized by an arbitrary factor. The solid line in (b) is the Gd atomic scattering factor $f_0+f'(E)$, obtained from absorption measurements (see text).

Figure 5 shows polarized Raman spectra of $GdAl_3$ for GA1–GA4 surfaces (see Sec. II A) in selected scattering geometries at room temperature. All the five expected Raman modes were clearly observed, according to the following symmetry assignment: E_{1g} mode at 83 cm^{-1}, A_{1g} mode at 292 cm^{-1}, and E_{2g} modes at 100, 198, and 270 cm^{-1}, which are summarized in Table II. Figure 5 also shows an extra peak at 216 cm^{-1} with unidentified symmetry (indicated by an arrow). This mode is observed with enhanced intensity for the polished xz surface of GA1 and is not seen in the fresh broken xy surfaces of GA4 and GA5. Thus, it appears to be a Raman-forbidden phonon, which is observed due to crystalline imperfections possibly enhanced by the surface polishing. In this context, we should mention that the Raman-active phonons are slightly narrower for GA4 and GA5 with respect to all other surfaces, confirming the better structural quality of these surfaces. On the other hand, the phonons are still fairly narrow for all other surfaces, indicating that the degree of structural disorder in the polished or naturally grown surfaces is not excessively large.

Figures 6(a)–6(f) show the T dependence of the frequencies of the observed modes for surfaces GA1–GA3. The lines in the figures give the expected conventional behavior using the expression reported by Balkanski *et al.*[32] For these samples, clear frequency anomalies take place below T^* $\sim$50 K for the modes at 102, 276, and 298 cm^{-1}. Also, the sign and magnitude of the anomalies are surface dependent [see Figs. 6(b), 6(e), and 6(f)]. The Raman-forbidden peak at $\sim$220 cm^{-1} also shows anomalous behavior below T^* [see Fig. 6(d)]. Figures 7(a)–7(d) show the frequency behavior for the observed modes in the GA4 and GA5 fresh bulk samples. In opposition to what has been observed for GA1–GA3, no clear frequency anomaly could be detected at T^*, within our sensitivity. No change in the phonon behavior was observed at the long-range magnetic ordering temperature, T_N=18 K, for any of the studied surfaces. Besides, the T dependence of all phonon linewidths (not shown) did not reveal any anomaly at T^* for any of the surfaces.

IV. DISCUSSION

Despite the extensive search for resonant magnetic Bragg peaks performed throughout the reciprocal space, no magnetic contribution to the x-ray intensities was observed below T_N=18 K. Possible reasons are as follows: (i) the propagation vector $\vec{\tau}$ of the magnetic structure was not covered by the one-dimensional (1D) and two-dimensional searches in the reciprocal space described in Table I and Fig. 2; (ii) a relatively weak resonance for magnetic x-ray diffraction takes place in this compound and the magnetic intensities became too weak to be observed within our sensitivity; (iii) the strong and intricate scattering from extended crystalline defects (see Fig. 2) may mask the intrinsic magnetic scattering; (iv) the antiferromagnetic structure might have a propa-

TABLE II. Factor group analysis of the $GdAl_3$ crystal structure (space group $P6_3/mmc$) and the experimentally observed phonon modes (in cm^{-1}).

Atoms	Wyckoff notation	Site symmetry	Irreducible representation
Gd	$2c$	D_{3h}^1	$A_{2u}+B_{1g}+E_{1u}+E_{2g}$
Al	$6h$	C_{2v}^1	$A_{1g}+A_{2g}+A_{2u}+B_{1g}+B_{1u}+B_{2u}+E_{1g}+2E_{1u}+2E_{2g}+E_{2u}$
	Total		$A_{1g}+A_{2g}+2A_{2u}+2B_{1g}+B_{1u}+B_{2u}+E_{1g}+3E_{1u}+3E_{2g}+E_{2u}$
		Mode classifications	
			$\Gamma_{Raman}=A_{1g}+E_{1g}+3E_{2g}$
			$\Gamma_{IR}=A_{2u}+2E_{1u}$
			$\Gamma_{acoustic}=A_{2u}+E_{1u}$
			$\Gamma_{silent}=A_{2g}+2B_{1g}+B_{1u}+B_{2u}+E_{2u}$
		Observed phonon modes (300 K)	
A_{1g}	E_{1g}	E_{2g}	
292	83	100	
		198	
		270	

gation vector $\vec{\tau}=(0,0,0)$ and therefore the magnetic Bragg peak positions would coincide with the charge Bragg peaks. Concerning the last possibility, we note that due to multiple scattering and to the simultaneous symmetry-lowering transition below T_N (see below), even the (3 3 1) and presumably other symmetry-forbidden reflections show non-negligible intensities due to charge scattering, perhaps overwhelming the possible magnetic contribution. Therefore, neutron diffraction could be the most suitable technique in this case to resolve the magnetic structure of $GdAl_3$, despite the inconveniently high neutron absorption cross section for Gd ions without isotopic purification.

Even considering the nonmagnetic origin of the observed (3 3 1) reflection, it reveals interesting physics for $GdAl_3$. The scaling between the E dependence of the structure factor of this reflection and $[f_0+f'(E)]$ (Gd) [see Fig. 4(b)] indicates that this scattering arises entirely from the Gd charge sector and therefore reflects a symmetry lowering associated with Gd displacements. This result indicates a static spin-lattice coupling due to an exchange striction effect. The reduced symmetry appears to be a manifestation of the frus-

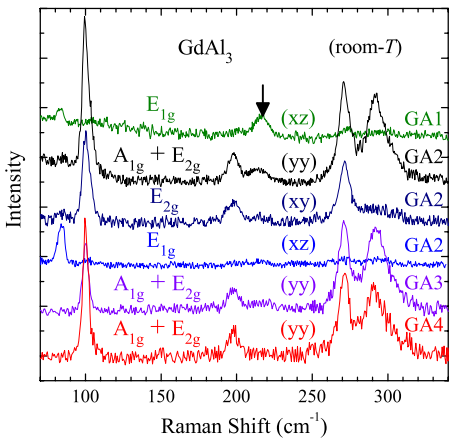

FIG. 5. (Color online) Room temperature polarized Raman scattering spectra in polished (GA1), natural (GA2 and GA3), and fresh broken (GA4) faces of $GdAl_3$ single crystals at selected polarizations.

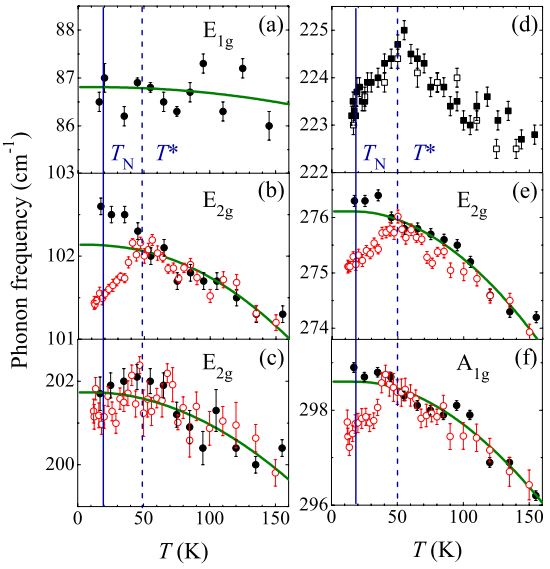

FIG. 6. (Color online) [(a)–(c), (e), and (f)] T dependency of the frequencies of the observed Raman peaks for samples GA2 (○) and GA3 (●). (E_{1g}: xz polarization; E_{2g}, A_{1g}: yy polarization). (d) T dependence of two different measurements for the mode at ~220 cm^{-1} in GA1, using xz polarization. The solid vertical lines represent the antiferromagnetic transition temperature, T_N, while the dashed line indicates T^*, the temperature below which anomalous phonon behavior is observed. The curves displayed in solid lines give the fit to a conventional behavior (Ref. 32).

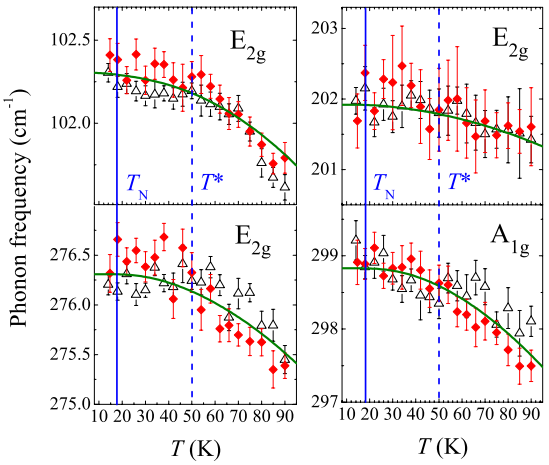

FIG. 7. (Color online) T dependency of the frequencies of the observed Raman peaks for the fresh bulk samples GA4 (open symbols) and GA5 (filled symbols).

trated magnetism of this compound since the Gd atomic displacements may, in principle, enhance the fulfilled magnetic interactions and weaken the frustrated ones, such as observed in other magnetically frustrated materials.[33,34]

Note that as Gd $4f^7$ is a half-filled and therefore spherically symmetrical shell with $L=0$, the spin-lattice coupling in $GdAl_3$ is not associated with magnetostriction or any other effect arising from the orbital degree of freedom. Thus, this coupling must arise entirely from the the dependence of the exchange energy with the atomic positions (exchange striction). The exchange coupling in $GdAl_3$ is arguably due to the RKKY mechanism, i.e., the Gd localized spins are coupled by the conduction electrons. For an isotropic metal with spherical Fermi surface, the RKKY exchange coefficient J_{ij} is proportional to $F(2k_F|\vec{R}_i-\vec{R}_j|)$, where $F(x)=(x\cos x-\sin x)/x^4$, k_F is the magnitude of the Fermi wave vector, and $\vec{R}_i$ is the position of the ith magnetic ion.[16] Thus, the magnetic energy depends explicitly on the positions of the magnetic ions and not of the intervening ions. This position dependence is much smoother than for direct exchange of superexchange mechanisms; therefore, the spin-lattice coupling is expected to be weaker in insulators. We should mention that there is an additional, implicit, dependence of the magnetic energy on displacements of both magnetic and nonmagnetic ions in the RKKY Hamiltonian, arising from the Fermi wave vector. Such dependence is not expected to be significant for good metals but may be important for materials with low density of charge carriers.

Thus, only Gd displacements are expected to contribute to the spin-lattice coupling in intermetallic $GdAl_3$. In fact, concerning the static spin-lattice coupling revealed in the synchrotron x-ray diffraction data, the evidence shown in Fig. 4(b) and discussed above indicates that the symmetry reduction below T_N is purely associated with Gd displacements, consistent with our expectations.

Our Raman results taken in old surfaces consistently point to a characteristic temperature $T^*\sim 50$ K, separating two quite different regimes. Above T^*, the phonon frequency as a function of temperature is essentially surface independent (see Fig. 6), in clear contrast with the behavior below T^*. Fresh broken GA4 and GA5 did not present clear frequency anomalies at T^*, while the old surfaces GA1–GA3, subjected to some possible lattice defects, reveal anomalies in some of the phonon frequencies below $\sim T^*$. This observation points to an extrinsic effect. On the other hand, our polarization analysis showed that most of the observed modes, with the possible exception of the one at 216 cm^{-1}, are associated with the $GdAl_3$ crystal structure. Therefore, frequency anomalies should be a consequence of a cooperative phenomenon occurring within this structure, even for possibly defective surfaces such as GA1–GA3. Thus, we suggest that the phonon anomalies at T^* are reflecting the change of an intrinsic property of $GdAl_3$, where the role of the possible defects in GA1–GA3 would be to enhance or create a mechanism to couple the optical phonons to the intrinsic effect occurring below T^* and not to create the effect itself. It is therefore valid to search for bulk physical properties of $GdAl_3$ with significant changes below ~ 50 K. In fact, it corresponds to the temperature below which the g value obtained by EPR deviates from 2.00 and its linewidth starts to increase most rapidly.[20] These are indications of strong short-range spin correlations below T^*, ascribed to the magnetic frustration in this compound. Weaker spin correlations have been found up to $\theta_{CW}\sim -90$ K, as seen in Fig. 1(b) and reported in Refs. 20 and 21.

On the basis of the above, it is reasonable to ascribe the phonon anomalies at T^* to a spin-phonon coupling. In fact, similar anomalies in the paramagnetic phase due to this mechanism have been previously observed in other magnetically frustrated materials, such as $ZnCr_2O_4$ (Ref. 15) and RMn_2O_5.[11] However, the spin-phonon coupling arguably observed here is presumably enhanced by the possible presence of defects at the vicinity of polished and/or old surfaces of $GdAl_3$. In fact, such defects may promote charge localization in the near-surface region, potentially incrementing the dependence of the Fermi wave vector k_F on small displacements of Gd and Al ions. This might enhance the spin-phonon coupling in the RKKY Hamiltonian, which would depend on the specific surface conditions, explaining our Raman data.

On the basis of the above interpretation for our Raman results, it is interesting to note that no phonon anomaly was observed at $T_N=18$ K for any of the studied surfaces, signaling that the short-range spin correlation function remains nearly unchanged at the long-range magnetic ordering temperature. This may be a consequence of the fairly large frustration ratio $|\theta_{CW}|/T_N\sim 4.9$, leading to a fully spin-correlated state for $T_N<T<T^*$.

V. CONCLUSIONS

In summary, we investigated the static first-order and the dynamical second-order spin-lattice coupling in the frustrated intermetallic compound $GdAl_3$ by means of synchrotron x-ray diffraction and Raman spectroscopy, respectively. A lattice symmetry reduction, associated with Gd ions alone, was observed below $T_N=18$ K, in accordance with expectations for the RKKY Hamiltonian. Also, frequency anomalies

in some of the Raman phonon modes were observed in old and/or polished surfaces below $T^* \sim 50$ K, which was ascribed to an enhancement of the spin-phonon coupling mechanism due to the presence of defects. This interpretation of our Raman results leads to the conclusion that a fully spin-correlated state without long-range order takes place immediately above T_N. Our observations may stimulate systematic investigations of the weak but fundamentally interesting spin-lattice coupling in metallic systems.

ACKNOWLEDGMENTS

We are indebted to S. B. Oseroff for helpful discussions. This work was supported by Fapesp and CNPq, Brazil, and NSF-DMR-0600742, USA. LNLS is acknowledged for beam time.

*egranado@ifi.unicamp.br

[1] *Physics of Manganites*, edited by T. A. Kaplan and S. D. Mahanti (Springer, New York, 1999).
[2] See, for example, S.-W. Cheong and M. Mostovoy, Nat. Mater. **6**, 13 (2007) and references therein.
[3] A. De Campos, D. L. Rocco, A. M. G. Carvalho, L. Caron, A. A. Coelho, S. Gama, L. M. Da Silva, F. C. G. Gandra, A. O. Dos Santos, L. P. Cardoso, P. J. Von Ranke, and N. A. De Oliveira, Nat. Mater. **5**, 802 (2006).
[4] C. Azimonte, J. C. Cezar, E. Granado, Q. Huang, J. W. Lynn, J. C. P. Campoy, J. Gopalakrishnan, and K. Ramesha, Phys. Rev. Lett. **98**, 017204 (2007).
[5] W. Baltensperger and J. S. Helman, Helv. Phys. Acta **41**, 668 (1968).
[6] E. Granado, A. García, J. A. Sanjurjo, C. Rettori, I. Torriani, F. Prado, R. Sanchez, A. Caneiro, and S. B. Oseroff, Phys. Rev. B **60**, 11879 (1999).
[7] E. Granado, P. G. Pagliuso, J. A. Sanjurjo, C. Rettori, M. A. Subramanian, S.-W. Cheong, and S. B. Oseroff, Phys. Rev. B **60**, 6513 (1999).
[8] E. Granado, N. O. Moreno, H. Martinho, A. García, J. A. Sanjurjo, I. Torriani, C. Rettori, J. J. Neumeier, and S. B. Oseroff, Phys. Rev. Lett. **86**, 5385 (2001).
[9] A. B. Souchkov, J. R. Simpson, M. Quijada, H. Ishibashi, N. Hur, J. S. Ahn, S. W. Cheong, A. J. Millis, and H. D. Drew, Phys. Rev. Lett. **91**, 027203 (2003).
[10] T. Rudolf, K. Pucher, F. Mayr, D. Samusi, V. Tsurkan, R. Tidecks, J. Deisenhofer, and A. Loidl, Phys. Rev. B **72**, 014450 (2005).
[11] A. F. García-Flores, E. Granado, H. Martinho, R. R. Urbano, C. Rettori, E. I. Golovenchits, V. A. Sanina, S. B. Oseroff, S. Park, and S.-W. Cheong, Phys. Rev. B **73**, 104411 (2006).
[12] C. J. Fennie and K. M. Rabe, Phys. Rev. Lett. **96**, 205505 (2006).
[13] J. Laverdière, S. Jandl, A. A. Mukhin, V. Yu. Ivanov, V. G. Ivanov, and M. N. Iliev, Phys. Rev. B **73**, 214301 (2006).
[14] J. Hemberger, T. Rudolf, H.-A. Krug von Nidda, F. Mayr, A. Pimenov, V. Tsurkan, and A. Loidl, Phys. Rev. Lett. **97**, 087204 (2006).
[15] A. B. Sushkov, O. Tchernyshyov, W. Ratcliff II, S. W. Cheong, and H. D. Drew, Phys. Rev. Lett. **94**, 137202 (2005).
[16] M. A. Ruderman and C. Kittel, Phys. Rev. **96**, 99 (1954); T. Kasuya, Prog. Theor. Phys. **16**, 45 (1956); K. Yosida, Phys. Rev. **106**, 893 (1957).
[17] J. A. Chilton and B. R. Coles, J. Alloys Compd. **183**, 385 (1992).
[18] A. S. Edelstein, R. L. Holtz, D. J. Gillespie, M. Rubinstein, J. Tyson, R. A. Fisher, and Norman E. Phillips, Phys. Rev. B **37**, 7877 (1988).
[19] A. S. Edelstein, R. L. Holtz, D. J. Gillespie, R. A. Fisher, and N. E. Phillips, J. Magn. Magn. Mater. **63**, 335 (1987).
[20] B. R. Coles, S. Oseroff, and Z. Fisk, J. Phys. F: Met. Phys. **17**, L169 (1987).
[21] K. H. J. Buschow and J. F. Fast, Phys. Status Solidi **16**, 467 (1966).
[22] S. P. S. Porto and J. F. Scott, Phys. Rev. **157**, 716 (1967).
[23] E. Granado, P. G. Pagliuso, C. Giles, R. Lora-Serrano, F. Yokaichiya, and J. L. Sarrao, Phys. Rev. B **69**, 144411 (2004).
[24] E. Granado, B. Uchoa, A. Malachias, R. Lora-Serrano, P. G. Pagliuso, and H. Westfahl, Jr., Phys. Rev. B **74**, 214428 (2006).
[25] N. W. Ashcroft and N. D. Mermin, in *Solid State Physics* (Thomson Learning, 1976).
[26] J. H. N. van Vucht and K. H. J. Buschow, J. Less-Common Met. **10**, 98 (1965).
[27] Marina A. Zhuravleva, K. Kasthuri Rangan, Melissa Lane, Paul Brazis, C. R. Kannewurf, and Mercouri G. Kanatzidis, J. Alloys Compd. **316**, 137 (2001).
[28] E. E. Havinga, J. Less-Common Met. **41**, 241 (1975).
[29] K. Nordlund, J. Appl. Phys. **91**, 2978 (2002); K. Nordlund, T. H. Metzger, A. Malachias, L. Capello, P. Calvo, A. Claverie, and F. Cristiano, *ibid.* **98**, 073529 (2005).
[30] Y. Waseda, in *Anomalous X-Ray Scattering for Materials Characterization* (Springer, New York, 2002).
[31] D. L. Rousseau, R. P. Bauman, and S. P. S. Porto, J. Raman Spectrosc. **10**, 253 (1981).
[32] M. Balkanski, R. F. Wallis, and E. Haro, Phys. Rev. B **28**, 1928 (1983).
[33] A. Huq, J. F. Mitchell, H. Zheng, L. C. Chapon, P. G. Radaelli, K. S. Knight, and P. W. Stephens, J. Solid State Chem. **179**, 1136 (2006).
[34] G. R. Blake, L. C. Chapon, P. G. Radaelli, S. Park, N. Hur, S.-W. Cheong, and J. Rodriguez-Carvajal, Phys. Rev. B **71**, 214402 (2005).